

T Tauri Stars: Physical Parameters and Evolutionary Status

K. N. Grankin

Crimean Astrophysical Observatory, Nauchny, Crimea, 298409 Russia

konstantin.grankin@mail.ru

Abstract

Long-term homogeneous photometry for 35 classical T Tauri stars (cTTS) in the Taurus–Auriga star-forming region (Tau-Aur SFR) has been analyzed. Reliable effective temperatures, interstellar extinctions, luminosities, radii, masses, and ages have been determined for these cTTS. The physical parameters and evolutionary status of 35 cTTS from this work and 34 weak-line T Tauri stars (wTTS) from previous studies have been compared. The luminosities, radii, and rotation periods of low-mass ($0.3\text{--}1.1 M_{\odot}$) cTTS are shown to be, on average, greater than those of low-mass wTTS, in good agreement with the evolutionary status of these two subgroups. The mean age of the younger subgroup of wTTS from our sample (2.3 Myr) essentially coincides with the mean duration of the protoplanetary disk accretion phase (2.3 Myr) for a representative sample of low-mass stars in seven young stellar clusters. The accretion disk dissipation time scale for the younger subgroup of cTTS (age < 4 Myr) in the Tau-Aur SFR is shown to be no greater than 0.4 Myr, in good agreement with the short protoplanetary disk dissipation time scale that is predicted by present-day protoplanetary disk evolution models.

Key words: *stars, pre-main-sequence stars, T Tauri stars – physical properties, evolutionary status.*

INTRODUCTION

The Taurus–Auriga complex of molecular clouds is one of the nearest and well-studied SFRs. The relatively low interstellar extinction, the small distance (about 140 pc), the presence of a rich population of young (1–10 Myr) low-mass stars, and the absence of ionizing radiation and winds from young massive stars make it an ideal object for studying the formation of solar-mass stars and testing theoretical stellar evolution models.

By 2008 the population of known young stars in the Tau–Aur SFR had numbered 364 objects (Kenyon et al. 2008). According to the empirical classification scheme proposed by Lada (1987) and André et al. (1993), these objects form an approximate age sequence from

protostars surrounded by thick gas and dust envelopes (Class 0 and I objects) to T Tauri stars (TTS) with circumstellar disks (Class II objects) and to TTS without accretion disks (Class III objects). The last two groups include cTTS with strong emission lines and significant infrared (IR) and ultraviolet (UV) excesses and wTTS with insignificant excesses.

The evolution of TTS within the first several million years is determined by strong magnetic fields (~ 2 kG) and circumstellar disks. On the one hand, the magnetic fields and outer deep convective envelopes of protostars are responsible for the existence of extended cool spots, hot facular fields, excess chromospheric and coronal emissions, short flares, and other manifestations of solar-type activity that are observed among wTTS. On the other hand, the magnetic fields play a key role in the complex processes of interaction between the central star and its surrounding disk, which lead to a redistribution of the angular momentum of the star–disk system and to the development of magnetospheric accretion processes typical for cTTS.

Present-day magnetospheric accretion models show that the stellar magnetic field acts on the disk at a distance of several stellar radii from the stellar surface. The inner disk material ionized by stellar radiation moves toward the star along magnetic field lines with the free-fall velocity, creating hot spots on the stellar surface. Part of the ionized gas is ejected back to form a wind and jets (see, e.g., Petrov 2003 for a review).

The phenomena of solar activity and magnetospheric accretion processes produce X-ray, UV, optical, and IR excess emissions that change the shape of the continuum and veil the photospheric spectral lines. Some of the young systems seen in the protoplanetary disk plane can exhibit irregular or quasi-periodic fadings attributable to the eclipses of much of the stellar surface by the warped inner disk edge, as with AA Tau and related objects (Alencar et al. 2010).

All these phenomena and processes complicate significantly the determination of basic physical parameters for young stars (such as the luminosity, radius, mass, age, accretion rate, etc.) and their evolutionary status, which is very important for testing various models for the evolution of young stars.

Attempts to determine the physical parameters of tens of TTS in the Tau–Aur SFR have been made in a number of papers (see, e.g., Cohen and Kuhl 1979; Strom et al. 1989; Valenti et al. 1993; Kenyon and Hartmann 1995; Hartigan et al. 1995; Gullbring et al. 1998; White and Ghez 2001; Furlan et al. 2006; Rebull et al. 2010; Furlan et al. 2011; Andrews et al. 2013; Herczeg and Hillenbrand 2014).

All these studies were performed properly and systematically. Nevertheless, the differences in some of the physical parameters for the same stars are very large in the above papers. One of the main reasons for these differences is the difficulty of estimating the interstellar extinction (A_V). Hartigan et al. (1995) point out that the main source of uncertainty in the A_V estimates is the variability of the magnitude, color, and veiling of some TTS. They cite the star DR Tau, whose veiling varies between 6.4 and 20 and whose V -band photometric variability exceeds one magnitude, as an example. Another example is the heavily veiled star DO Tau, in which the excess continuum dominates the photospheric flux. The authors argue that the contribution of the veiling continuum in the V band reaches 80%. Thus, the color of this object will be considerably bluer than that of the same star without optical veiling. A significant scatter in extinction estimates is observed even in the case of TTS with weak accretion. For example, for the weakly veiled star DN Tau, Gullbring et al. (1998) provided $A_V \sim 0.2$, Kenyon and Hartmann (1995) estimated $A_V \sim 0.5$, and Hartigan et al. (1995) obtained $A_V \sim 1.1$.

Ingleby et al. (2013) provide published extinction estimates for 13 cTTS and point out that the values of A_V obtained by different authors for the same star differ significantly. For half of the objects from Ingleby et al. (2013), the scatter in A_V reaches ± 0.5 , which can lead to an

uncertainty of one order of magnitude in estimating the accretion rate and some other physical parameters of cTTS.

To attempt to minimize the uncertainties in the spectral type, extinction, and veiling of cTTS, one can apply the method of simultaneously fitting all three parameters. Recently, such simultaneous fitting has been applied for cTTS in the Tau–Aur SFR (Fischer et al. 2011; McClure et al. 2013; Herczeg and Hillenbrand 2014). Nevertheless, the scatter in A_V estimates not only did not decrease but even increased to ± 0.8 . For the three objects DF Tau, DO Tau, and DG Tau, the differences in A_V estimates reached ± 1.2 , ± 1.6 , and ± 2.7 , respectively. Herczeg and Hillenbrand (2014) rightly note that the significant uncertainties in A_V and other parameters of cTTS introduce scepticism in our ability to use the main properties of cTTS to test theories of star formation and pre-main-sequence evolution.

Quite realistic estimates of A_V and other parameters of TTS can be obtained if long-term homogeneous multicolor photometry is used for these objects. Analysis of a large number of magnitude estimates in several bands (for example, in U , B , V , and R) allows one to determine the maximum and minimum brightnesses with a high accuracy and to establish reliable color–magnitude relations. In turn, knowledge of these parameters of the photometric behavior for TTS makes it possible to accurately estimate the color excesses that are attributable either to accretion processes, or to cool extended spots, or to variable circumstellar extinction. Allowance for these excesses enables one to determine the magnitudes and colors that correspond to the intrinsic TTS photosphere and, hence, to calculate reliable values of A_V and other parameters of young stars.

Such long-term homogeneous photometric observations of 34 cTTS and 40 wTTS in the Tau–Aur SFR had been performed as part of the ROTOR program at the Maidanak Observatory in Uzbekistan for almost twenty years (1984–2006). The results of these observations and their statistical analysis were presented in Grankin et al. (2007, 2008). Subsequently, Grankin (2013a) analyzed long-term observations for 28 wTTS and 60 wTTS candidates in the Tau–Aur SFR. This analysis showed that more than 60 objects from this sample exhibit periodic light variations attributable to spotted rotational modulation. To minimize the influence of photometric variability on the A_V estimate and the luminosity L_{bol} , we used the maximum brightness (V_{max}) and the corresponding $(V - R)$ color, which is virtually insensitive to the possible presence of hot spots and the manifestations of chromospheric activity (see Gullbring et al. 1998). We hypothesized that the visible wTTS surface was least covered with spots at the time of maximum light. Therefore, its brightness and color correspond most closely to a true photosphere. Because of this, we calculated reliable extinctions, luminosities, radii, masses, and ages for 74 wTTS and related objects in the Tau–Aur SFR. Based on these data, we refined the evolutionary status of these objects (Grankin et al. 2013b) and investigated the relationship between activity and rotation (Grankin 2013c).

This paper is a logical continuation of our studies begun in Grankin (2013a–2013c). Our goals are: (1) to obtain reliable estimates of the basic physical parameters for 35 cTTS in the Tau–Aur SFR based on published homogeneous long-term photometric data (Grankin et al. 2007); (2) to compare the physical parameters of cTTS and wTTS; and (3) to refine their evolutionary status.

DETERMINATION OF STELLAR PROPERTIES

The estimates of the luminosity, radius, mass, age, and other stellar parameters of cTTS depend primarily on how accurately the effective temperature (T_{eff}) and interstellar extinction (A_V) have been determined.

Effective Temperature

The sample presented in this paper includes 35 cTTS from the Tau–Aur SFR. Homogeneous long-term photometric data (Grankin et al. 2007) are available for the overwhelming majority of objects. Information about the cTTS spectral types was taken mainly from Furlan et al. (2011) and, only in a few cases, from Fischer et al. (2011), Nguyen et al. (2009), Güdel et al. (2007), and Johns-Krull et al. (2000). These spectral types were converted to temperatures using the temperature calibration from Tokunaga (2000). The arguments for choosing this calibration and the corresponding uncertainties in T_{eff} were discussed in detail in Grankin (2013a). Note only that before choosing Tokunaga’s calibration, we analyzed several different temperature scales from Cohen and Kuhi (1979), de Jager and Nieuwenhuijzen (1987), Bessell (1991), Kenyon and Hartmann (1995), Tokunaga (2000), Luhman et al. (2003), and Herczeg and Hillenbrand (2014). The temperature scales were compared with the experimental data on the temperatures and spectral types of 43 main-sequence dwarfs from Torres et al. (2010). Since these stars are components of noninteracting eclipsing systems, their basic physical parameters are known with an accuracy of at least $\pm 3\%$. A statistical analysis showed that the experimental data from Torres et al. (2010) agree best with the temperature calibration from Tokunaga (2000) with a standard deviation of ± 90 K. The temperature calibrations mentioned above are presented in Table 1.

If we use the temperature calibration from Tokunaga (2000) and take the uncertainty in the spectral classification as ± 1 subclass, then the corresponding uncertainty in T_{eff} will be ± 50 , ± 100 , ± 195 , ± 90 , and ± 160 K for G1–G6, G7–K1, K2–K6, K7–M0, and M1–M6 stars, respectively. The last row in Table 1 provides the rms deviation that characterizes the scatter between the experimental data from Torres et al. (2010) and the temperature calibration corresponding to a given column. The values calculated by spline interpolation are italicized.

Interstellar Extinction

As has been noted in the Introduction, cTTS have considerable X-ray, UV, optical, and IR excesses that change the shape of the continuum and make it more difficult to calculate the interstellar extinction A_V and, hence, the bolometric luminosity L_{bol} and all of the remaining stellar parameters. On the one hand, the $U - B$ and $B - V$ colors become considerably bluer in cTTS due to the presence of hot facular fields, excess chromospheric emission, short flares, and hot spots located at the base of accretion columns. On the other hand, the colors become slightly redder due to the presence of extended cool spots, variable circumstellar extinction, additional warm disk emission, and, in some cases, due to partial eclipses of the stellar surface by the warped inner disk edge. Therefore, it is highly problematic to determine the magnitudes and colors corresponding to the cTTS photosphere (see, e.g., Petrov and Kozak 2007). However, the actual value of A_V cannot be estimated without knowing these quantities. To illustrate the aforesaid, we presented the $V - R$ color – V magnitude relation in Fig. 1 for one wTTS (V827 Tau) and one cTTS (DL Tau). Both objects have the same spectral type K7 and $T_{eff} = 4040$ K. The photometric data are represented by the gray dots. The $(V - R)_o$ color of a standard star of the corresponding spectral type K7 is marked by the vertical line.

In the case of V827 Tau (Fig. 1a), the main source of its photometric brightness and color variability is the presence of dark photospheric spots. Model calculations show that the observed color–magnitude relation is best described by dark spots with a temperature lower than the photospheric temperature by 1000 K that cover about 67% of the entire stellar surface. The modeling results are represented by the dash–dotted line. A detailed description of the model calculations can be found in Grankin (1998). Since the visible surface of V827 Tau at

Table 1. Temperature calibrations

Sp. T.	CK79 ^a	B91 ^b	deJN87 ^c	KH95 ^d	L03 ^e	HH14 ^f	T00 ^g
G0	5902	6000	5943	6030		5930	5930
G1	5834	<i>5917</i>		5945			<i>5876</i>
G2	5768	<i>5833</i>	5794	5860		5690	5830
G3				5830			<i>5786</i>
G4			5636	5800			5740
G5	5662	<i>5583</i>	<i>5554</i>	5770		5430	<i>5687</i>
G6	5445	5500		5700			5620
G7				5630			<i>5535</i>
G8			5309	5520		5180	<i>5438</i>
G9				5410			<i>5337</i>
K0	5236	<i>5167</i>	5152	5250		4870	5240
K1	5105	<i>5083</i>	4989	5080		<i>4790</i>	<i>5145</i>
K2	4955	5000	<i>4808</i>	4900		4710	5010
K3	4775	<i>4750</i>	4688	4730		<i>4543</i>	<i>4801</i>
K4	4581	4500	4539	4590		<i>4377</i>	4560
K5	4395		4406	4350		4210	4340
K6	4198			4205			<i>4166</i>
K7	3999	4000	4150	4060		4020	4040
K8							<i>3954</i>
K9			3936				<i>3883</i>
M0	3917	3800	3837	3850		3900	3800
M1	3681	3650	3664	3720	3705	3720	3680
M2	3499	3500	3524	3580	3560	3560	3530
M3	3357	3350	3404	3470	3415	3410	3380
M4	3228	3150	3289	3370	3270	3190	3180
M5	3119	3000	3170	3240	3125	2980	3030
M6	2958	2800	3034	3050	2990	2860	2850
SD	±99K	±111K	±136K	±134K	±140K	±242K	± 90K

Notes. a – Cohen and Kuhi, 1979; b – Bessell, 1991; c – de Jager and Nieuwenhuijzen, 1987; d – Kenyon and Hartmann, 1995; e – Luhman et al., 2003; f – Herczeg and Hillenbrand, 2014; g – Tokunaga, 2000.

maximum light is least covered with spots, its maximum brightness and the corresponding color marked by the large white circle correspond most closely to a true photosphere. The dashed line indicates the brightness level that corresponds to a true stellar photosphere observed through absorbing interstellar clouds (V'_{ph}). It is these values that are used to calculate the interstellar reddening A_V (black arrow) and to determine the dereddened magnitude V^o_{ph} (black circle).

In the case of the cTTS DL Tau (Fig. 1b), the brightness and color variations are attributable primarily to the presence of a hot spot at the base of an accretion column. For this reason, the minimum brightness and the corresponding color (white circle), when the hot spot is located on the invisible side of the star, will correspond (to a first approximation) to a true photosphere. Our modeling shows that the observed color–magnitude relation corresponds most closely to a hot spot with a temperature of ~ 10000 K and an area of $\sim 1.7\%$ of the entire stellar surface (dash–dotted line). Obviously, in the case of cTTS, not the maximum brightness and the corresponding color (as in the case of wTTS) but the minimum brightness and the

corresponding color should be used to obtain realistic interstellar extinction estimates (black arrow). However, the source of the cTTS photometric variability is not only the hot accretion spot but also variable circumstellar extinction (as in AA Tau), dark spots, hot facular fields, and some other processes (see above). Therefore, the choice of the brightness (V'_{ph}) and the corresponding color that correspond most closely to a “quiet” cTTS photosphere and that could be used to determine a realistic value of A_V is highly ambiguous. Below, we present the next algorithm to determine A_V .

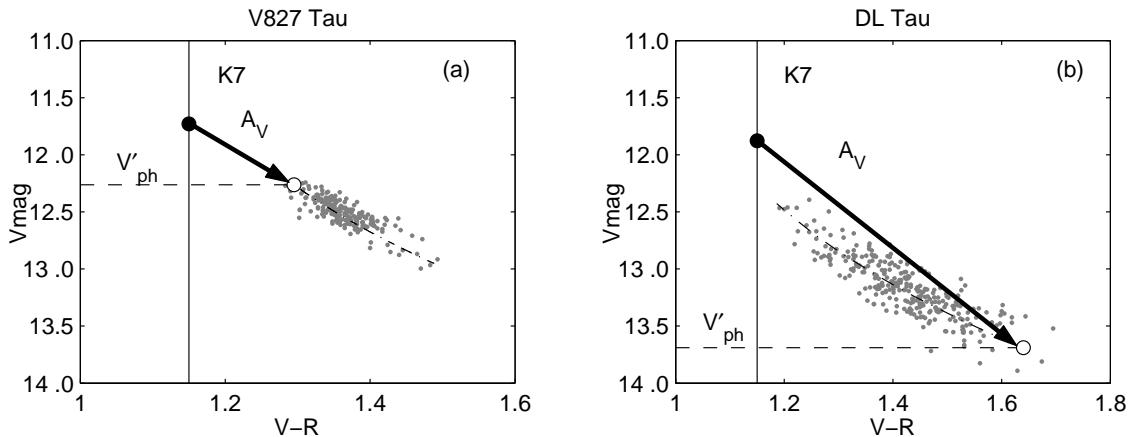


Figure 1: $V - R$ color - V magnitude relation for wTTS (a) and cTTS (b). The photometric data are marked by the gray dots. The solid vertical line indicates the color of a standard dwarf star of the same spectral type K7 without interstellar extinction. The large white circle corresponds to the presumed magnitude V'_{ph} and color $(V - R)_{ph}$ that refer to the “quiet” stellar photosphere. The dashed horizontal line indicates the brightness level V'_{ph} . The large black circle indicates the dereddened magnitude and color of the star. The black arrow indicates the interstellar reddening A_V . The modeling results that describe best the photometric behavior of the objects are represented by the dash-dotted line. The observed color-magnitude relation for the wTTS V827 Tau corresponds to the model with dark spots with a temperature lower than the photospheric temperature by 1000 K and an area of 67% of the entire stellar surface. In contrast, the photometric behavior of the cTTS DL Tau can be explained by the presence of a hot spot with a temperature of ~ 10000 K and an area of $\sim 1.7\%$ of the entire stellar surface.

To take into account the possible contribution of the emission from a hot spot and facular areas, we used long-term homogeneous BVR photometry from Grankin et al. (2007). Analysis of the color-magnitude diagrams showed that all cTTS from our sample exhibit considerable blue excesses (estimates of the color excess E_{U-B} , $E_{B-V} < 0$). Figure 2a presents the $B - V$ color - V magnitude relation for the star CI Tau, which shows signatures of noticeable accretion. The $(B - V)_o$ color of a standard star of the corresponding spectral type K7 is marked by the vertical line. The actual color-magnitude relation is marked by the dash-dotted line. It can be seen from the figure that many of the magnitudes and colors are located to the left of the vertical line, where $E_{B-V} < 0$. Obviously, these magnitudes and $B - V$ colors are attributable to the accretion processes, and they cannot be used to estimate A_V . Nevertheless, we can assume that the brightness level at which the blue excess disappears ($E_{B-V} = 0$) corresponds to a normal stellar photosphere observed through interstellar clouds. This brightness level (V'_{ph}) is marked by the horizontal dashed line and the white circle.

Given the upper photospheric brightness limit V'_{ph} and the $V - R$ color-magnitude relation, we can estimate the color excess E_{V-R} attributable only to the interstellar extinction (Fig. 2b). We propose to use such a value that corresponds to V'_{ph} (marked by the vertical dotted line) as the photospheric $(V - R)_{ph}$ color. The photospheric brightness and the corresponding $(V - R)_{ph}$

color chosen in this way are marked by the white circle. According to the proposed technique, the color excess due to the interstellar extinction is estimated as $E_{V-R} = 0.39$. Finally, the interstellar extinction was calculated from the well-known formula $A_V = 3.7E_{V-R}$ for the V and R bands of the Johnson (1968) photometric system.

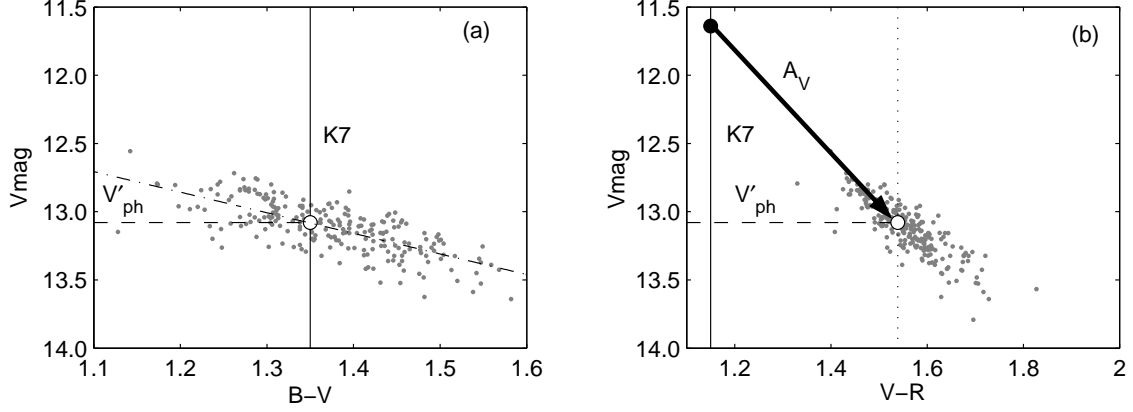


Figure 2: (a) $B - V$ color - magnitude relation for the cTTS CI Tau. The designations are the same as those in Fig. 1. The gray dots represent the photometric data. The solid vertical line indicates the $B - V$ color of a standard dwarf star of the same spectral type as that of the cTTS under study but without interstellar extinction. The dash-dotted line is a linear fit to the photometric data. The dashed horizontal line indicates the brightness level of the cTTS under study (V'_{ph}) for which the color excess $E_{B-V} = 0$. (b) $V - R$ Color-magnitude relation for the cTTS CI Tau. The solid vertical line indicates the $V - R$ color of a standard dwarf star of the same spectral type as that of the cTTS under study but without interstellar extinction. The dotted vertical line indicates the $(V - R)_{ph}$ color of the cTTS under study that corresponds to V'_{ph} . The large white circle corresponds to the magnitude V'_{ph} and $(V - R)_{ph}$ color that are free from the accretion excess and that are used to calculate the interstellar extinction A_V (black arrow). The large black circle indicates the dereddened magnitude and color of the star.

To check the reliability of our extinction estimates, we compared them with the published values of A_V . Information regarding the published values of A_V was taken from 18 different papers, with the references to most of them being given in the Introduction. Figure 3 compares our values of the extinction with those from several publications with which good agreement is observed. Our values of A_V agree best with the published estimates from Cohen and Kuhi (1979), Strom et al. (1989), and Kenyon and Hartmann (1995). These authors used the $V - R$ or $V - I$ colors to measure the extinction. As an example, our values of A_V are compared with those from Strom et al. (1989) in Fig. 3a. There is an excellent overlap between our values and the results of these authors, with a shift of -0.08^m and a standard deviation of 0.48^m . The agreement with the data from Cohen and Kuhi (1979) (a shift of -0.01^m and a standard deviation of 0.57^m) and from Kenyon and Hartmann (1995) (a shift of -0.06^m and a standard deviation of 0.57^m) is slightly poorer.

The differences with the extinction estimates from Rebull et al. (2010) and Furlan et al. (2011) obtained from near-IR photometry ($J - H$ or $J - K$) are more significant and systematic. For example, the mean shift and standard deviation of our values of A_V relative to those from Rebull et al. (2010) are $+1.25^m$ and 3.75^m , respectively. When our values of A_V are compared with those from Furlan et al. (2011), the situation is slightly better: the mean shift is $+0.59^m$ and the standard deviation is 1.08^m (see Fig. 3b). In both cases, analysis of the near-IR photometry gives considerably higher extinction estimates than those obtained at optical wavelengths.

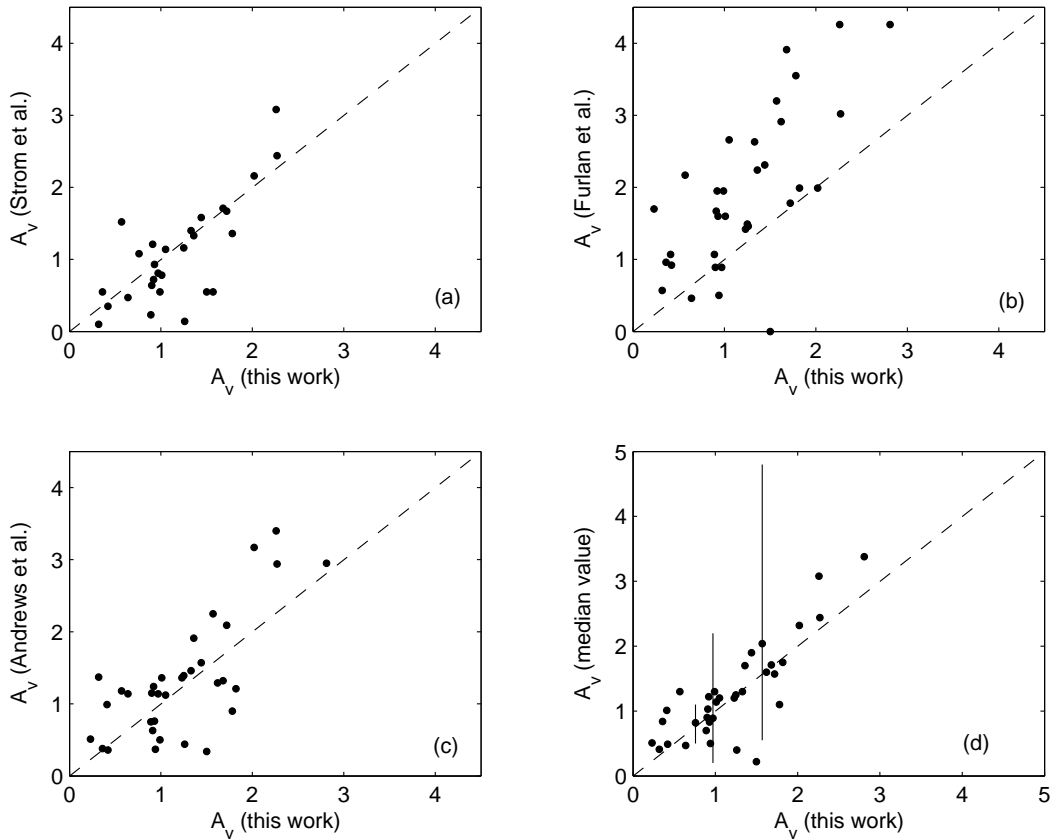


Figure 3: Comparison of A_V from this paper with its values from Strom et al. (1989) (a), Furlan et al. (2011) (b), Andrews et al. (2013) (c), and the median values of A_V (d). The three vertical bars indicate a typical scatter between the maximum and minimum values of A_V for three different objects: DI Tau ($\Delta A_V = 0.60^m$), DE Tau ($\Delta A_V = 2.0^m$), and RY Tau ($\Delta A_V = 4.3^m$). Despite the large differences between individual published A_V estimates, the median values agree excellently with our extinction estimates, with a shift of $+0.08^m$ and a standard deviation of 0.18^m .

Andrews et al. (2013) applied a method for estimating the extinction and luminosity by fitting spectral templates of stellar photosphere models to the actual spectral energy distributions of cTTS. Our values of A_V are compared with those from Andrews et al. (2013) in Fig. 3c. The agreement with our data is good, with a shift of $+0.17^m$ and a standard deviation of 0.31^m . Unfortunately, comparison with other works showed very significant discrepancies in the A_V estimates. For example, analysis of 12 works showed that the maximum and minimum values of A_V for CW Tau differ by 5.1^m (from 1.8 to 6.9); the differences for DG Tau, RY Tau, DO Tau, and DD Tau reach 4.4 , 4.3 , 4.2 , and 3.9^m , respectively. For most of the remaining objects from our sample, the differences between the maximum and minimum values of A_V are close to 2^m . Taking this fact into account, we gathered all of the independent A_V determinations from the literature for our objects and calculated the median values of the extinction. Figure 3d compares our extinction estimates with these median values of A_V . The vertical bars indicate a typical scatter between the maximum and minimum values of A_V for three different objects: DI Tau ($\Delta A_V = 0.60^m$), DE Tau ($\Delta A_V = 2.0^m$), and RY Tau ($\Delta A_V = 4.3^m$). Despite the large differences between individual published A_V estimates, the median values agree excellently with our extinction estimates, with a shift of $+0.08^m$ and a standard deviation of 0.18^m . Thus, we think that our technique provides a good way for estimating reliable values of the interstellar extinction.

Luminosity and Radius

The bolometric luminosity (L_{bol}) was calculated using a well-known formula: $\log(L_*/L_\odot) = -0.4(V_{max} - A_V + BC + 5 - 5 \log r - 4.72)$, where BC is the bolometric correction from Hartigan et al. (1994), and r is the mean distance to the Tau–Aur SFR (140 pc). The various sources of errors in the L_{bol} estimates were discussed in Grankin (2013a). The most significant errors can be caused by the possible presence of a secondary component and the uncertainty in the adopted distance to the Tau–Aur SFR.

About 70 multiple systems in the Tau–Aur SFR are known to date (Harris et al. 2012). In our sample consisting of 35 cTTS, 13 objects are components of binary or multiple systems. The magnitude difference for the components of three objects is more than 1.8^m , and the errors in L_{bol} are insignificant for them. For the remaining 10 objects, we can overestimate L_{bol} in the worst case by a factor of 2 if the magnitudes of the components are assumed to be the same.

An equally serious problem can be associated with the uncertainty in the distance. According to several accurate individual trigonometric parallaxes (an error of $\sim 0.4\%$) obtained through VLBI measurements (Loinard et al. 2007; Torres et al. 2009, 2012), the mean distance to the Tau–Aur SFR is $d = 140.6 \pm 13.6$ pc. This value is in good agreement with its previous estimates ($d = 140 \pm 20$ pc). Thus, an uncertainty in the distance of ± 20 pc can lead to an error in $\log L_{bol}$ of the order of ± 0.13 dex.

The stellar radii were determined by two methods. First, we estimated the radii (R_{bol}) using T_{eff} and L_{bol} . Second, we used the ratio from Kervella and Fouqué (2008). These authors obtained an empirical relation between the angular diameters of the nearest dwarfs and their visible colors. They showed that the angular diameter could be calculated with an accuracy of at least 5%. We calculated the stellar radii (R_{KF}) by using the Kervella–Fouqué calibration and by assuming the mean distance to the Tau–Aur SFR to be 140 pc. R_{bol} is plotted against R_{KF} in Fig. 4. The estimates of the radii are in good agreement with the mean ratio $\langle R_{KF}/R_{bol} \rangle = 0.964 \pm 0.017$.

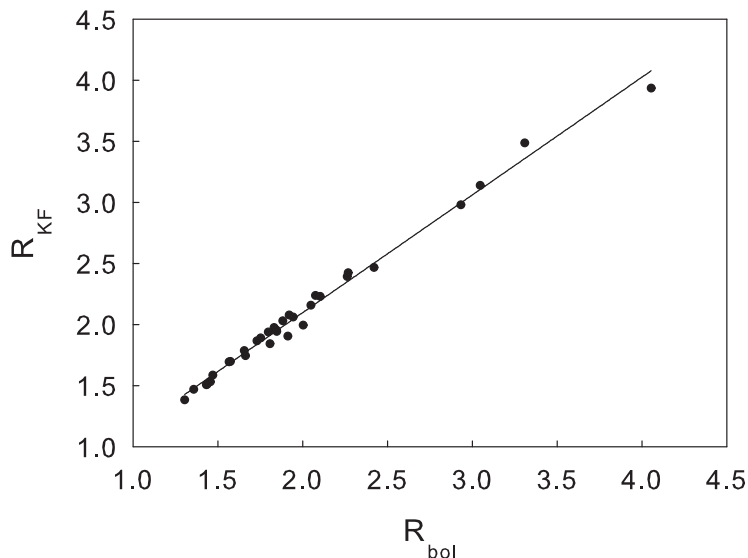


Figure 4: Comparison of the stellar radii R_{bol} obtained using L_{bol} and T_{eff} with the radii R_{KF} calculated from the Kervella–Fouqué relation. The estimates of the radii are in good agreement with the mean ratio $\langle R_{KF}/R_{bol} \rangle = 0.964 \pm 0.017$.

Mass and Age

To determine the masses and ages of the stars from our sample, we used the grid of evolutionary tracks from Siess et al. (2000) computed for pre-mainsequence (PMS) stars. The Hertzsprung–Russell (HR) diagram for 35 cTTS is presented in Fig. 5a. For comparison, Fig. 5b shows the HR diagram for 17 well-known wTTS (filled squares) and 17 new wTTS (open squares) from Grankin (2013b). The inaccuracies in the mass and age estimates are attributable to the uncertainties in T_{eff} and L_{bol} adopted in this paper and depend on the object’s position on the HR diagram. The error in the mass is $\pm 0.1 M_{\odot}$ for the stars on convective tracks and $\pm 0.2 M_{\odot}$ for the objects on radiative tracks. The relative error in the age is of the order of $\pm 1 - 4$ Myr.

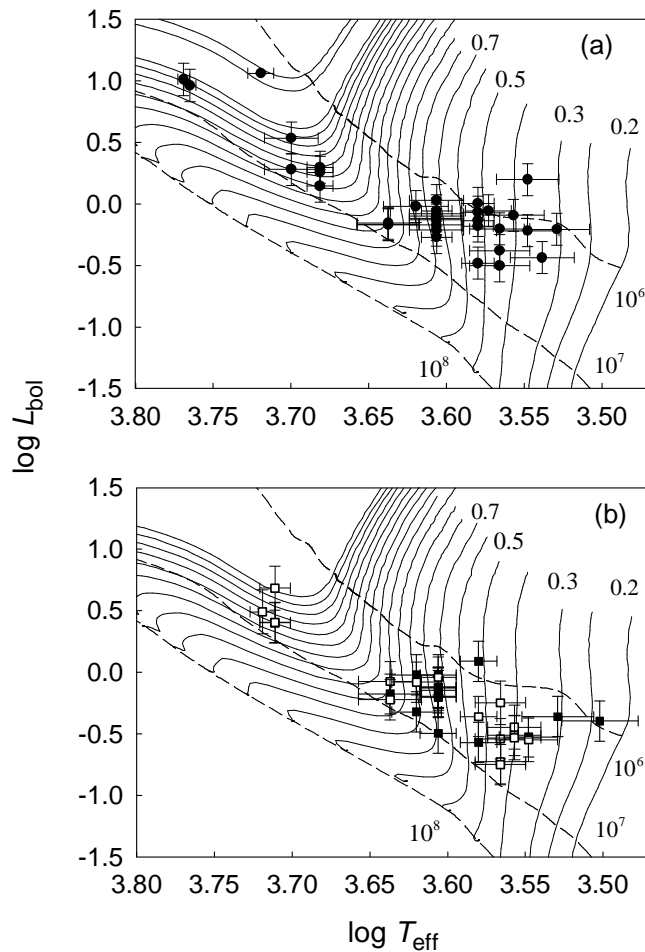


Figure 5: HR diagram for cTTS (a) and wTTS (b). The filled circles are cTTS, the filled squares are well-known wTTS, and the open squares are new wTTS. The errors indicate the $\pm 1\sigma$ uncertainty for L_{bol} and T_{eff} . The solid lines are the evolutionary tracks calculated with $Y = 0.277$ and $Z = 0.02$ for stars with masses of 0.2, 0.25, 0.3, 0.4, 0.5, 0.6, 0.7, 0.8, 0.9, 1.0, 1.1, 1.2, 1.3, 1.4, 1.5, 1.6, 1.7, 1.8, 1.9, 2.0, 2.5, and 2.7 M_{\odot} . The dashed lines are the isochrones for ages of 10^6 , 10^7 , and 10^8 yr.

It can be seen from Fig. 5 that the overwhelming majority of cTTS and wTTS occupy the same region on the HR diagram that corresponds to the range of masses from 0.3 to 1.1 M_{\odot} . Only three wTTS and seven cTTS are on the evolutionary tracks corresponding to more massive PMS stars with masses from 1.4 to 2.0 M_{\odot} . The star T Tau, the TTS prototype, is at the very top of the HR diagram between the tracks that correspond to PMS stars with masses of 2.5 and 2.7 M_{\odot} .

The basic cTTS parameters and the intermediate data used to calculate them are presented in Table 2. Since the same photometric database and the same technique were used to determine the physical parameters of 35 cTTS from this paper and 34 wTTS from Grankin (2013b), the systematic errors in these parameters must be minimal for the two samples of young stars. Therefore, comparing the parameters and evolutionary status of cTTS and wTTS from the Tau–Aur SFR is of considerable interest.

EVOLUTIONARY STATUS

The main difference between the cTTS and wTTS is that the cTTS have accretion disks, while the wTTS are devoid of such disks or at least their inner regions. For this reason, the wTTS must rotate faster and be slightly older than the cTTS. If this assumption is valid and the wTTS are actually older objects, then their luminosities and radii must be smaller than those of the cTTS. To test this assumption, we constructed the corresponding histograms.

Figure 6 shows the distributions (histograms) of luminosities and radii for both cTTS (Figs. 6a and 6c) and wTTS (Figs. 6b and 6d). In both samples of stars, there are several objects with luminosities $> 1.5L_{\odot}$. If we neglect these objects and select the best Gaussians for stars with luminosities in the range from 0.18 to $1.23 L_{\odot}$, then we will find that the mean cTTS luminosity ($0.70L_{\odot} \pm 0.20L_{\odot}$) is slightly greater than the mean wTTS luminosity ($0.56L_{\odot} \pm 0.27L_{\odot}$). Accordingly, for the overwhelming majority of objects with radii in the range from 1 to $2.5 R_{\odot}$, we find that the mean cTTS radius ($1.83R_{\odot} \pm 0.29R_{\odot}$) is slightly larger than the mean wTTS radius ($1.59R_{\odot} \pm 0.30R_{\odot}$).

The distributions (histograms) of ages and masses for the cTTS and wTTS are presented in Fig. 7. It follows from the figure that the age and mass distributions for both subgroups have a complex shape, and they cannot be classified as simple unimodal (in this case, they must have had one pronounced peak) or uniform (in this case, the histograms would contain an approximately equal number of values in each bin). The age and mass distributions (histograms) presented in Fig. 7 are closest in their shape to bimodal ones. Unfortunately, we can say nothing about the significance of the bimodal shape of the distributions based on a small data sample (35 cTTS and 34 wTTS). Reliably determining the shape of a complex distribution, including the bimodal one, requires a considerably larger volume of input data: from 400 to 2000 values (see, e.g., Novitskii and Zograf 1985). Nevertheless, analysis of Figs. 7a and 7b shows that the age distribution has a bimodal structure for both subgroups: young stars with ages of 1–4 Myr and objects with ages of 5–10 Myr.

The approximation using two Gaussians gives two maximum values of about 1.9 ± 0.9 and 6.1 ± 1.3 Myr for the cTTS and 2.3 ± 0.8 and 7.0 ± 1.5 Myr for the wTTS. Thus, the mean age of the older cTTS subgroup is smaller than the mean age of the analogous wTTS subgroup by 0.9 Myr. At the same time, the mean age of the younger cTTS subgroup is smaller than the mean age of the analogous wTTS subgroup by 0.4 Myr. Since the difference between the mean ages of the younger cTTS and wTTS subgroups is smaller than the relative error in the age (see the previous section), we estimated the significance of this difference based on Student’s t-test or, more specifically, the significance was calculated from the confidence interval and the smallest significant difference (SSD). Both methods showed the difference between the mean ages of the younger cTTS and wTTS subgroups to be statistically insignificant at the 90% confidence level.

Table 2. Basic cTTS parameters and the intermediate data used to calculate them. The masses and ages were estimated in comparison with the theoretical models and tracks calculated by Siess et al. (2000)

Name	Sp. type	Ref.	T_{eff} , K	V'_{ph}	$V - R$	E_{V-R}	A_V	L_{bol} , L_{\odot}	R , R_{\odot}	M , M_{\odot}	t , 10^6 yr
AA Tau	K7	1	4040	12.94	1.40	0.25	0.92	0.54	1.47	0.77	2.09
BP Tau	K7	1	4040	12.38	1.39	0.24	0.89	0.88	1.88	0.75	3.16
CI Tau	K7	1	4040	13.08	1.54	0.39	1.44	0.76	1.75	0.74	2.49
CW Tau	K3	1	4801	12.14	1.35	0.53	1.95	1.85	1.94	1.50	4.90
CX Tau	M2.5	1	3455	13.72	1.65	0.10	0.36	0.37	1.66	0.34	1.66
CY Tau	M1	2	3680	13.66	1.74	0.34	1.26	0.63	1.92	0.45	1.31
DD Tau	M3.5	1	3280	14.83	2.13	0.48	1.78	0.62	2.26	0.27	0.29
DE Tau	M1.5	1	3605	13.23	1.71	0.26	0.97	0.81	2.27	0.41	0.99
DF Tau	M2	1	3530	12.65	1.77	0.27	0.99	1.58	3.31	0.37	0.13
DG Tau A	K6	1	4166	12.88	1.51	0.44	1.62	0.95	1.85	0.87	2.41
DH Tau	M1	1	3680	13.73	1.56	0.16	0.57	0.31	1.36	0.45	2.92
DI Tau	M0	3	3800	12.84	1.49	0.21	0.76	0.66	1.84	0.53	1.52
DK Tau	K7	1	4040	12.88	1.51	0.36	1.33	0.83	1.83	0.74	2.22
DL Tau	K7	1	4040	13.69	1.64	0.49	1.82	0.61	1.57	0.75	3.39
DM Tau	M1	1	3680	14.35	1.81	0.41	1.50	0.42	1.57	0.45	2.01
DN Tau	M0	1	3800	12.38	1.39	0.11	0.42	0.73	1.94	0.53	1.35
DO Tau E ^a	M0	1	3800				2.27	1.01	2.25	0.52	0.97
DR Tau	K5	1	4340	12.72	1.32	0.33	1.23	0.68	1.43	1.10	7.06
DS Tau	K5	1	4340	12.42	1.24	0.25	0.93	0.68	1.44	1.10	7.06
GG Tau A	K7	4	4040	12.18	1.40	0.25	0.91	1.07	2.08	0.72	1.62
GI Tau	K7	1	4040	13.03	1.52	0.37	1.36	0.74	1.73	0.74	2.57
GK Tau	K7	1	4040	12.59	1.42	0.27	1.01	0.80	1.80	0.74	2.33
GM Aur	K7	1	4040	12.08	1.24	0.09	0.32	0.68	1.66	0.75	2.89
HP Tau AB ^b	K3	3	4801				2.26	1.40	1.77	1.39	6.90
HQ Tau	K2	1	5010	12.23	1.50	0.76	2.81	3.43	2.42	1.88	4.02
IP Tau	M0	1	3800	13.05	1.34	0.06	0.23	0.33	1.30	0.54	3.77
IQ Tau ^b	M0.5	3	3740				1.25	0.88	2.20	0.51	1.06
RW Aur	K3	1	4801	11.16	1.06	0.24	0.87	1.69	1.85	1.50	6.09
RY Tau	G1	1	5876	9.55	0.94	0.42	1.57	10.28	3.05	1.93	5.93
SU Aur	G2	4	5830	9.01	0.77	0.24	0.90	9.18	2.93	1.88	6.40
T Tau	K0	1	5240	9.83	1.11	0.47	1.72	11.51	4.05	2.64	2.06
UX Tau A	K2	5	5010	10.68	0.91	0.17	0.64	1.91	1.81	1.55	8.62
UY Aur	M0	1	3800	12.84	1.56	0.28	1.05	0.86	2.10	0.52	1.13
V1079 Tau	K5	1	4340	11.87	1.10	0.11	0.41	0.70	1.46	1.10	6.78
XZ Tau	M2	1	3530	14.39	1.95	0.45	1.68	0.61	2.05	0.37	1.19

1 – Furlan et al. 2011; 2 – Fischer et al. 2011; 3 – Güdel et al. 2007; 4 – Nguyen et al. 2009; 5 – Johns-Krull et al. 2000.
a – A_V and L_{bol} from Gullbring et al. 1998; b – A_V and L_{bol} from Güdel et al. 2007.

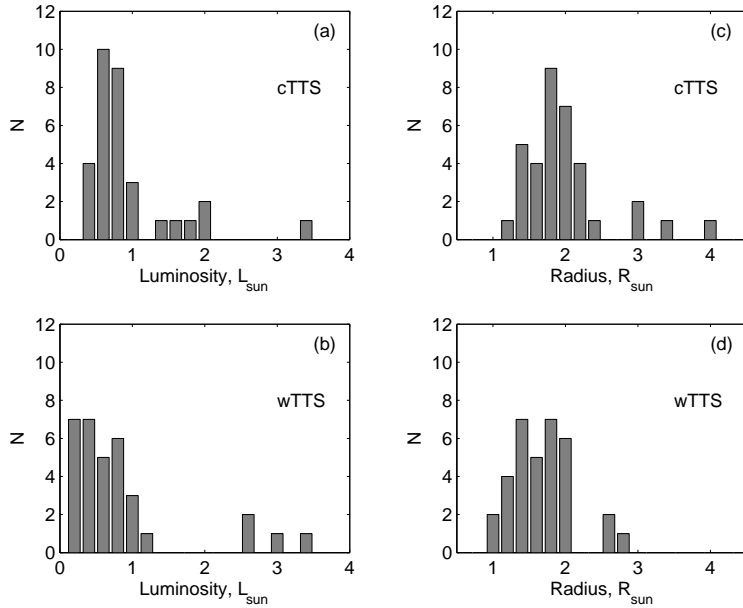


Figure 6: Distributions of luminosities (a, b) and radii (c, d) for cTTS and wTTS.

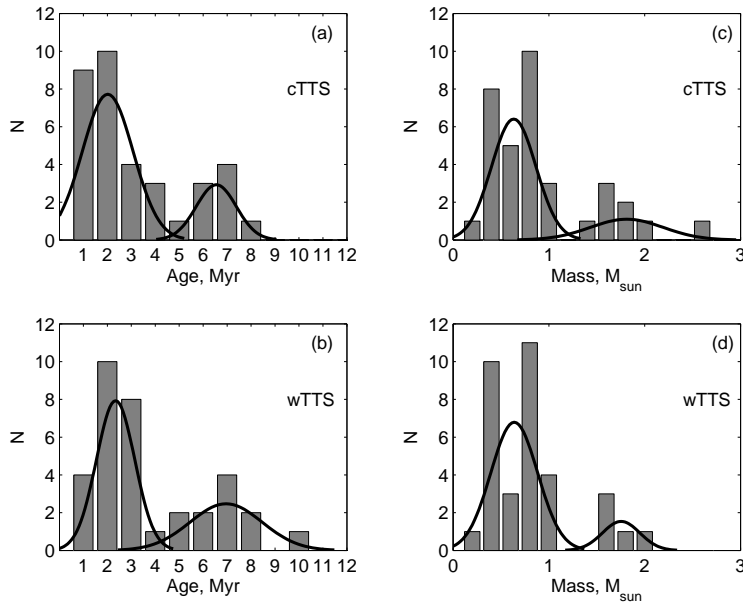


Figure 7: Distributions of ages (a, b) and masses (c, d) for cTTS and wTTS.

It may well be that the bimodal pattern of the age distribution is attributable to the selection effects in our data. A more representative sample of wTTS and cTTS should be analyzed. If the age distribution is actually bimodal, then there is reason to assert that the star formation process in the Tau–Aur SFR was more likely cyclic than continuous.

The approximation using two Gaussians for the cTTS and wTTS mass distributions allows two subgroups to be identified: a subgroup of stars with masses of $0.2\text{--}1.1 M_{\odot}$ and a subgroup of stars with masses of $1.4\text{--}2.6 M_{\odot}$ (see Figs. 7c and 7d, respectively). The mean masses of these two subgroups are 0.63 ± 0.23 and $1.81 \pm 0.38 M_{\odot}$ for the cTTS and 0.64 ± 0.23 and $1.75 \pm 0.19 M_{\odot}$ for the wTTS. It can be argued that the mass distributions for the cTTS and wTTS essentially coincide.

It has been noted above that we cannot determine the significance of the bimodal shape of the age and mass distributions due to the limited size of our sample. Nevertheless, our data on the mass distribution are consistent with the results of studying the initial mass function (IMF) in the Tau–Aur SFR. In contrast to other well-studied star-forming regions, the IMF for the Tau–Aur SFR has an unusual excess of stars with masses of 0.6–0.8 M_{\odot} and a clear deficit of objects with masses noticeably greater than 1 M_{\odot} (see, e.g., Luhman et al. 2009). Recent hydrodynamic simulations showed that the peculiar shape of the IMF could be a direct consequence of the unusual properties of the cores from which small groups of protostars were formed in the Tau–Aur SFR (Goodwin et al. 2004). Roughly 50% of the young stars formed in a core are ejected from the core to form a population of low-mass stars and brown dwarfs with a flat IMF. The remaining objects form multiple systems within the core, gradually accrete matter, and produce a population of intermediate-mass stars whose IMF peaks at $\sim 0.6\text{--}0.8 M_{\odot}$.

To compare the rotation of cTTS and wTTS, we selected objects with known rotation periods (Artemenko et al. 2012; Grankin 2013a), ages < 4 Myr, and masses in the range 0.2–1.1 M_{\odot} . As a result, the cTTS and wTTS samples contain 17 and 15 objects, respectively. The distributions of cTTS and wTTS rotation periods are presented in Figs. 8a and 8b, respectively. It follows from the figure that most of the cTTS (12 of 17) have rotation periods in the range from 5.5 to 8.1 days, three objects rotate with periods of 3.2–4.6 days, and only two stars have periods longer than 10 days. In contrast, among the wTTS there are only four objects with periods in the range from 5.5 to 8.1 days, and 60% of the stars have rotation periods in the range from 0.6 to 3.8 days. A statistical analysis showed that the mean cTTS and wTTS rotation periods are 6.98 ± 2.73 and 4.31 ± 2.56 days, respectively. The 95% confidence intervals for these mean values coincide and are equal to 1.3 days.

Our estimate of the mean age for the younger and larger wTTS subgroup (2.3 Myr) agrees excellently with the time at which the disk accretion phase ceases (2.3 Myr) from Fedele et al. (2010). These authors performed an optical spectroscopic survey of a representative sample of low-mass (K0–M5) stars from seven young stellar clusters (with ages from 2 to 30 Myr) and showed the disk accretion phase to cease in the overwhelming majority of these stars at an age of 2.3 Myr. This result is in good agreement with the present views of the evolutionary status of wTTS that lost their original disks through the accretion and formation of planetary systems.

The second result of our study suggests that the mean age of the younger and larger cTTS subgroup (1.9 Myr) is smaller than the mean age of the analogous wTTS subgroup in the Tau–Aur SFR by 0.4 Myr. Since all cTTS from our sample show signatures of accretion disks, while the wTTS lost their disks, it should be concluded that the accretion disks in the Tau–Aur SFR dissipate within a fairly short time interval, ~ 0.4 Myr. This result agrees well with the previous studies of the dissipation time scale for protoplanetary disks. They showed that the dissipation time scale for the original disk measured from the time at which the accretion process ceases does not exceed 0.5 Myr (see, e.g., Skrutskie et al. 1990; Wolk and Walter 1996; Cieza et al. 2007). The disk evolution models combining viscous accretion with photoevaporation successfully reproduce the fairly long lifetime of the original disk and the short disk dissipation time scale after the cessation of accretion (see, e.g., Alexander et al. 2006a, 2006b). A more detailed discussion of the evolution of a protoplanetary disk and the “two-time-scale” problem can be found in the review of Williams and Cieza (2011).

Comparison of the wTTS and cTTS rotation periods showed that the cTTS rotate, on average, more slowly (6.98 days) than do the wTTS (4.31 days). This result is consistent with the theoretical models that predict a decrease in the rotation period of PMS stars as they move toward the zero-age main sequence. Previous studies of the evolution of angular momentum

for PMS stars in the Tau–Aur SFR showed that most of the objects ceased to actively interact with their disks on a time scale from 0.7 to 10 Myr. Spin-up due to a rapid decrease in the moment of inertia is observed after disk dissipation (see, e.g., Grankin 2013b). Since the cTTS continue to actively interact with their accretion disks, they evolve with an almost constant angular velocity, and their rotation periods are grouped in a narrow range, from 5.5 to 8.1 days. In contrast, the wTTS lost their disks and rotate freely, remaining under the action of only the braking wind that carries away some part of the angular momentum. Therefore, the wTTS rotate faster, and many of them have rotation periods in the range from 0.6 to 3.8 days.

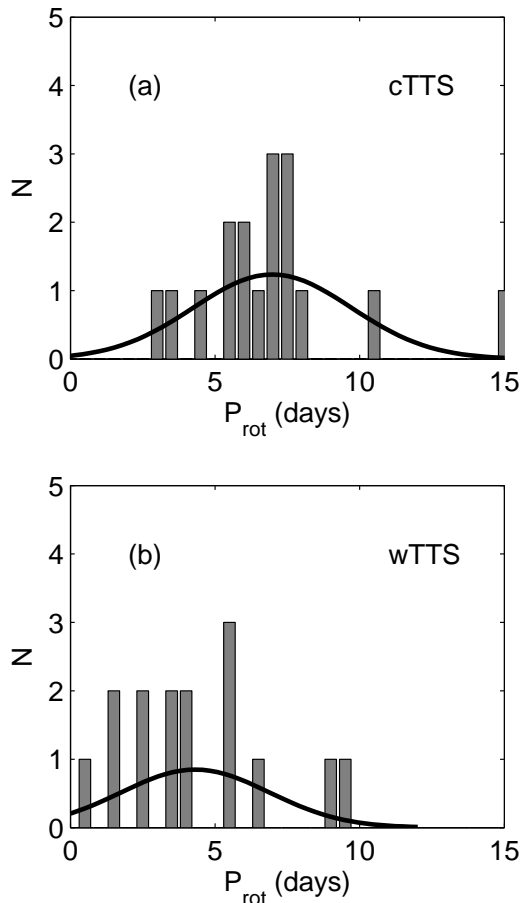


Figure 8: Distributions of rotation periods for cTTS (a) and wTTS (b).

CONCLUSIONS

Based on published homogeneous long-term photometric data (Grankin et al. 2007), we calculated reliable effective temperatures, interstellar extinctions, luminosities, radii, masses, and ages for 35 cTTS in the Tau–Aur SFR. T_{eff} were determined using the temperature calibration from Tokunaga (2000). The errors in T_{eff} can reach ± 50 , ± 100 , ± 195 , ± 90 , and ± 160 K for G1–G6, G7–K1, K2–K6, K7–M0, and M1–M6 stars, respectively.

Our analysis of the homogeneous long-term BVR photometry allowed the brightness level of each cTTS at which the blue excess attributable to the accretion processes disappears ($E_{B-V} = 0$) to be estimated. This brightness level (V'_{ph}) corresponds best to a normal stellar photosphere. To calculate the interstellar extinction A_V , we used the $(V - R)_{ph}$ color that corresponded to

V'_{ph} . These extinction estimates were compared with those from 18 different papers. Our values of A_V were shown to agree best with the published estimates from Cohen and Kuhi (1979), Strom et al. (1989), and Kenyon and Hartmann (1995). In contrast, significant systematic differences are observed for A_V from Rebull et al. (2010) and Furlan et al. (2011), where the extinction was calculated using near-IR photometry. Our extinction estimates were shown to agree excellently with the median values of A_V calculated using all the published values of this quantity.

We calculated the stellar bolometric luminosity L_{bol} by assuming all cTTS to be at the mean distance of the Taurus–Auriga SFR (140 pc), except for T Tau itself and HP Tau, whose more accurate distances are known from special studies. We showed that the actual scatter of distances to the Tau–Aur SFR (± 20 pc) could lead to an error in $\log L_{bol}$ of the order of ± 0.13 dex.

The stellar radii were calculated by two methods: using L_{bol} and $T_{eff}(R_{bol})$ and using the Kervella–Fouqué ratio (R_{KF}). The R_{bol} and R_{KF} estimates were shown to be in excellent agreement with the mean ratio $\langle R_{KF}/R_{bol} \rangle = 0.964 \pm 0.017$.

The masses and ages were determined using a grid of evolutionary tracks from Siess et al. (2000). The error in the mass for the stars on convective and radiative tracks is $\pm 0.1 M_\odot$ and about $\pm 0.2 M_\odot$, respectively. The relative error in the age is of the order of $\pm 1 - 4$ Myr. The overwhelming majority of cTTS (28 of 35 objects) have low masses in the range from 0.3 to $1.1 M_\odot$.

We compared the physical parameters and evolutionary status of 35 cTTS from this study and 34 wTTS with a reliable evolutionary status from Grankin (2013b). We identified two groups of objects among the wTTS and cTTS: low-mass ($0.2-1.1 M_\odot$) stars and stars with masses $1.4-2.6 M_\odot$. The low-mass cTTS were shown to have, on average, a high luminosity and a large radius than do the low-mass wTTS. In addition, the low-mass cTTS rotate, on average, more slowly ($\langle P_{rot} \rangle = 6.98$ days) than do the low-mass wTTS ($\langle P_{rot} \rangle = 4.31$ days). These results are in good agreement with the evolutionary status of the investigated objects.

Our analysis of the age distribution of stars showed that the cTTS and wTTS exhibit the same bimodal distribution: there are stars with ages 1–4 Myr and objects with ages 5–10 Myr. The mean age of the older cTTS subgroup (6.1 Myr) is smaller than the mean age of the analogous wTTS subgroup (7.0 Myr) by 0.9 Myr, while the mean age of the younger and more representative cTTS subgroup (1.9 Myr) is smaller than the mean age of the analogous wTTS subgroup (2.3 Myr) by 0.4 Myr. It may well be that the bimodal pattern of the age distribution is attributable to the selection effects.

The mean age of the younger subgroup of wTTS from our sample (2.3 Myr) essentially coincides with the mean duration of the accretion phase (2.3 Myr) determined by analyzing a representative sample of low-mass stars in the young stellar clusters σ Orionis, NGC 6231, NGC 6531, ASCC 58, NGC 2353, Collinder 65, and NGC 6664 (Fedele et al. 2010). This result is consistent with the present views of the evolutionary status of wTTS that lost their original disks through the accretion and formation of planetary systems.

The dissipation time scale of accretion disks in the Tau–Aur SFR was shown to be no greater than 0.4 Myr, in good agreement with the previous estimates of the protoplanetary disk dissipation time scale (see, e.g., Williams and Cieza 2011 for a review).

REFERENCES

1. S.H.P. Alencar, P.S. Teixeira, M.M. Guimarães, et al., *Astron. Astrophys.* **519**, A88 (2010).
2. R.D. Alexander, C.J. Clarke, and J.E. Pringle, *Mon. Not. R. Astron. Soc.* **369**, 216 (2006a).
3. R.D. Alexander, C.J. Clarke, and J.E. Pringle, *Mon. Not. R. Astron. Soc.* **369**, 229 (2006b).
4. P. André, D. Ward-Thompson, and M. Barsony, *Astrophys. J.* **406**, 122 (1993).
5. S.M. Andrews, K.A. Rosenfeld, A.L. Kraus, et al., *Astrophys. J.* **771**, 129 (2013).
6. S.A. Artemenko, K.N. Grankin, and P.P. Petrov, *Astron. Lett* **38**, 783 (2012).
7. M. Bessell, *Astron. J.* **101**, 662 (1991).
8. L. Cieza, D.L. Padgett, K.R. Stapelfeldt, et al., *Astrophys. J.* **667**, 308 (2007).
9. M. Cohen and L. Kuhl, *Astrophys. J. Suppl. Ser.* **41**, 743 (1979).
10. D. Fedele, M.E. van den Ancker, T. Henning, et al., *Astron. Astrophys.* **510**, 72 (2010).
11. W. Fischer, S. Edwards, L. Hillenbrand, et al., *Astrophys. J.* **730**, 73 (2011).
12. E. Furlan, L. Hartmann, N. Calvet, et al., *Astrophys. J. Suppl. Ser.* **165**, 568 (2006).
13. E. Furlan, K. L. Luhman, C. Espaillat, et al., *Astrophys. J. Suppl. Ser.* **195**, 3 (2011).
14. S.P. Goodwin, A.P. Whitworth, and D. Ward-Thompson, *Astron. Astrophys.* **419**, 543 (2004).
15. K.N. Grankin, *Astron. Lett.* **24**, 497 (1998).
16. K.N. Grankin, S.Yu. Melnikov, J. Bouvier, et al., *Astron. Astrophys.* **461**, 183 (2007).
17. K.N. Grankin, J. Bouvier, W. Herbst, et al., *Astron. Astrophys.* **479**, 827 (2008).
18. K.N. Grankin, *Astron. Lett.* **39**, 251 (2013a).
19. K.N. Grankin, *Astron. Lett.* **39**, 336 (2013b).
20. K.N. Grankin, *Astron. Lett.* **39**, 446 (2013c).
21. M. Güdel, K.R. Briggs, K. Arzner, et al., *Astron. Astrophys.* **468**, 353 (2007).
22. E. Gullbring, L. Hartmann, C. Briceño, et al., *Astrophys. J.* **492**, 323 (1998).
23. R.J. Harris, S.M. Andrews, D.J. Wilner, et al., *Astrophys. J.* **751**, 115 (2012).
24. P. Hartigan, S. Edwards, and L. Ghandour, *Astrophys. J.* **452**, 736 (1995).
25. G.J. Herczeg and L.A. Hillenbrand, *Astrophys. J.* **786**, 97 (2014).
26. L. Ingleby, N. Calvet, G. Herczeg, et al., *Astrophys. J.* **767**, 112 (2013).
27. C. de Jager and H. Nieuwenhuijzen, *Astron. Astrophys.* **177**, 217 (1987).
28. C.M. Johns-Krull, J.A. Valenti, and J.L. Linsky, *Astrophys. J.* **539**, 815 (2000).
29. H.L. Johnson, in *Nebulae and Interstellar Matter*, Ed. by B.M. Middlehurst and L.H. Aller (Univ. Chicago Press, Chicago, 1968), p. 167.
30. S.J. Kenyon and L. Hartmann, *Astrophys. J. Suppl. Ser.* **101**, 117 (1995).
31. S.J. Kenyon, M. Gómez, and B.A. Whitney, in *Handbook of Star Forming Regions*, Vol. 1: *The Northern Sky*, Ed. by Bo Reipurth (ASP Monograph, 2008), Vol. 4, p. 405.

32. P. Kervella and P. Fouqué, *Astron. Astrophys.* **491**, 855 (2008).
33. C.J. Lada, in *Star Forming Regions, Proceedings of the IAU Symp.* No. 115, Ed. by M. Peimbert and J. Jugaku (Cambridge Univ. Press, Cambridge, 1987), p. 1.
34. L. Loinard, R.M. Torres, A.J. Mioduszewski, et al., *Astrophys. J.* **671**, 546 (2007).
35. K.L. Luhman, J.R. Stauffer, A.A. Muench, et al., *Astrophys. J.* **593**, 1093 (2003).
36. K.L. Luhman, E.E. Mamajek, P.R. Allen, et al., *Astrophys. J.* **703**, 399 (2009).
37. M.K. McClure, N. Calvet, C. Espaillat, et al., *Astrophys. J.* **769**, 73 (2013).
38. D.C. Nguyen, R. Jayawardhana, M.H. van Kerkwijk, et al., *Astrophys.* **695**, 1648 (2009).
39. P.V. Novitskii and I.A. Zograf, *Estimation of Measurement Errors* (Energoatomizdat, Leningrad, 1985), p. 248 [in Russian].
40. P.P. Petrov, *Astrophysics* **46**, 506 (2003).
41. P.P. Petrov and B.S. Kozak, *Astron. Rep.* **51**, 500 (2007).
42. L.M. Rebull, D.L. Padgett, C.-E. McCabe, et al., *Astrophys. J. Suppl. Ser.* **186**, 259 (2010).
43. L. Siess, E. Dufour, and M. Forestini, *Astron. Astrophys.* **358**, 593 (2000).
44. M.F. Skrutskie, D. Dutkevitch, S.E. Strom, et al., *Astron. J.* **99**, 1187 (1990).
45. K.M. Strom, F.P. Wilkin, S.E. Strom, et al., *Astron. J.* **98**, 1444 (1989).
46. A. Tokunaga, *Allen's Astrophysical Quantities*, 4th ed., Ed. by A. N. Cox (Springer, New York, 2000), p. 143.
47. R.M. Torres, L. Loinard, A.J. Mioduszewski, et al., *Astrophys. J.* **698**, 242 (2009).
48. G. Torres, J. Andersen, and A. Gimenez, *Astron. Astrophys. Rev.* **18**, 67 (2010).
49. R.M. Torres, L. Loinard, A.J. Mioduszewski, et al., *Astrophys. J.* **747**, 18 (2012).
50. J.A. Valenti, G. Basri, and C.M. Johns, *Astron. J.* **106**, 2024 (1993).
51. R.J. White and A.M. Ghez, *Astrophys. J.* **556**, 265 (2001).
52. J.P. Williams and L.A. Cieza, *Ann. Rev. Astron. Astrophys.* **49**, 67 (2011).
53. S.J. Wolk and F.M. Walter, *Astron. J.* **111**, 2066 (1996).